Thin-Walled Structures 49 (2011) 437–447

Contents lists available at ScienceDirect

Thin-Walled Structures

journal homepage: www.elsevier.com/locate/tws

Thermoelastic dynamic stability of thin-walled beams with graded material properties

M.T. Piovan *, S.P. Machado

Centro de Investigaciones en Mecánica Teórica y Aplicada, Universidad Tecnológica Nacional - F.R.B.B., 11 de Abril 461, Bahía Blanca, BA, B8000LMI, Argentina

ARTICLE INFO

Article history:
Received 25 August 2010
Received in revised form
2 November 2010
Accepted 2 November 2010
Available online 4 December 2010

Keywords:
Dynamic stability
Thin walled beams
Thermal effects
Functionally graded materials

ABSTRACT

The dynamic stability of functionally graded thin-walled beams allowing for shear deformability is investigated in this article. The analysis is based on a model that has small strains and moderate rotations which are formulated through the adoption of a second-order non-linear displacement field. The beam is subjected to axial external dynamic loading. The model takes into account thermoelastic effects. The heat conduction equation is solved in order to characterize the temperature in the cross-sectional domain. Galerkin's and Bolotin's methods are employed with the scope to discretize the governing equations and to determine the regions of dynamic stability, respectively. Regions of stability are evaluated and expressed in non-dimensional form. The influence of the longitudinal vibration on the unstable regions is investigated. The numerical results show the importance of this effect when the forcing frequency approaches to the natural longitudinal frequency, obtaining substantially wider parametric stability regions. The effects of temperature gradients, shear flexibility and axial inertia, in beams with different cross-sections and different types of graded material are analyzed as well.

1. Introduction

Strategic and high technology industries, such as defense, aerospace or automotive industries are demanding new and advanced materials in order to increase the leadership in the development of high competitive goods. A few decades ago, designers claimed for new materials combining in a single sample, the best properties of different kind of materials. That is, for example, the stiffness, electrical conductivity and machinability of metals and the high strength, low density and high temperature resistance of ceramics. During the past 10–12 years these advanced materials are becoming no longer experimental sample of laboratories but a consistent reality. Functionally graded materials (FGM) are just an example of such advanced materials. In this type of materials the variation in percentage of phase constituents (normally ceramic and metal) can be arranged in such a way to create a new material with graded properties in spatial directions.

Many papers have been devoted to study shells and solids constructed with FGM such as the works carried out by a number of researchers [1–5]. There are many interesting approaches to analyze the mechanics of slender structures. Each approach offers different perspectives and useful modeling alternatives.

The recent works of Chakraborty et al. [6], Goupee and Vel [7], Ding et al. [8], Xiang and Yang [9] and Yang and Chen [10], among others, can be considered the most relevant for functionally graded straight beams. In these papers different laws defining the graded properties of the beams have been introduced. In this sense, the gradation laws can be defined in an exponential form or in a power law form or any other with "ad hoc" purposes. Many of the aforementioned papers introduce a three-dimensional or a two-dimensional complex model. On the other hand, there are quite a few papers devoted to study functionally graded thin-walled beams.

The works of Oh et al. [11,12] and Fazelzadeh and coworkers [13,14] are among the few papers devoted to the mechanics of thin-walled beams constructed with functionally graded materials. The scope of these papers has been mainly directed towards the analysis of rotating beams and secondarily to the analysis of thermo-elastic coupling effects associated with graded properties. Oh et al. [11,12] also focused their attention to the study of dynamic stability of cylindrical spinning beams.

The dynamic stability of elastic slender structures like beams, rods and columns, induced by parametric excitation has been investigated by many researchers. In the work of Nayfeh and Mook [15] extensive sources and literature on these topics can be found. The problems of dynamic stability have been thoroughly introduced and analyzed by Bolotin [16] for various classical structural elements, i.e. Bernoulli–Euler and Vlasov beam model among others. This last treatise provides useful tools for further studies and analysis on dynamic

* Corresponding author.
E-mail address: mpiovan@frbb.utn.edu.ar (M.T. Piovan).

0263-8231/$ - see front matter © 2010 Elsevier Ltd. All rights reserved.
doi:10.1016/j.tws.2010.11.002

Nomenclature

$\overline{A}_{ij},\overline{B}_{ij},\overline{D}_{ij}$	modified elastic shell coefficients
B, B_w	bi-moment and Wagner-effect related general force
c_i	coefficient for temperature-dependent properties
e, b, h	thickness, width and height of a cross section
E_i, E_o	Young's modulii at inner and outer surfaces
f	sub-index for properties of functionally graded material
J_{ij},J^{ρ}_{ij}	stiffness and inertia beam coefficients
K	exponent characterizing gradation of properties
M_y, M_z	bending moments
N_{ij}, M_{ij}	shell forces and moments
Q_x, Q_y, Q_z	axial and shearing beam forces
Q_{ij}	elastic constants
s, n	co-ordinates of the reference system in the wall
T	absolute temperature in Kelvin degrees
$\overline{T}_{ij}$	modified thermal shell coefficients
T_w, T_{sv}	flexo-torsional and pure torsion moments
u_o, v_o, w_o	displacements of the cross-sectional reference system
x, y, z	co-ordinates of the main reference system
y_o, z_o	Location of the shear center
M, **K**, **S**	matrices of mass, elastic stiffness and geometric stiffness
α_i,α_o	thermal expansion coefficient at inner and outer surfaces
ε_{Di}	generalized beam strains
κ_i,κ_o	thermal conductivity coefficient at inner and outer surfaces
ν_i,ν_o	Poisson coefficients at inner and outer surfaces
ρ_i,ρ_o	material density at inner and outer surfaces
$\sigma_{ij},\varepsilon_{ij}$	stresses and strain components
θ_y,θ_z	bending rotation parameters
ϕ_x,θ_x	twisting angle and warping parameter
Ω,ϖ	natural and forcing frequencies
$\mathcal{M}_i$	inertia forces on the beam

stability of slender structures. Some of these tools were employed by Machado and coworkers [17–19] to study different features in dynamic stability of thin-walled composite beams.

In spite of the practical interest and future potential of the thin-walled functionally graded beam structures, particularly in the context of aerospace and mechanical applications, the most of the contemporary available research is focused to characterize the dynamic behavior of beams with solid sections or, at least, beams modeled as long conical or cylindrical shells [20]. Under these circumstances, it appears that, to the best of authors' knowledge, there is a lack of research concerning to the problem of dynamic stability of thin-walled beams with graded properties and subjected to axial dynamic excitation. Then, considering this context, the present paper is devoted to analyze the patterns of dynamic stability for a given model of thin-walled beam considering full-shear deformability. The concept of full shear deformability is adopted [19,21,22] to mean the inclusion in a unified fashion shear stress/strain effects due to bending (the most common) and warping due to non-uniform torsion. Constitutive equations for functionally graded properties of beams subjected to thermal environment are developed and appropriately included in the model. The purpose of the present investigation is the characterization of the regions of dynamic stability of thin-walled functionally graded beams subjected to axial dynamic excitation and thermoelastic loadings as well.

The study of this paper is carried out employing a model that has small strains and moderate rotations which are formulated through the adoption of a second-order non-linear displacement field (see [17–19]). As a distinguish feature in comparison to other approaches (Oh et al. [11,12] for example), the model of the present paper has many non-linear effects (normally neglected by other authors) and takes into account the effect of longitudinal vibratory patterns and the interaction of the forced frequencies and the parametrically excited frequencies. Thus, as suggested in Bolotin [16] the differential equation of the longitudinal motion is solved in order to characterize the axial force in terms of forcing frequency and the static and dynamic parts of the forcing load; consequently this axial force is injected in the remaining equations. This leads to a reduced differential system. The boundaries of stability regions can be found by imposing in the reduced differential system periodic solutions that are parameterized with respect to the load forcing frequency.

The influence of different modeling features, such as thermo-elastic effects, shear deformation, longitudinal vibration coupling and different constitutive laws, on the shape of the unstable regions is extensively analyzed by means of parametric studies.

2. Model description

2.1. Basic assumptions and material featuring

In Fig. 1 one can see the structural model of a thin-walled beam. The points of the structural member are referred to a Cartesian co-ordinate system $\{\mathbf{O}:x,\overline{y},\overline{z}\}$ located at the centroid where the x-axis is parallel to the longitudinal axis of the beam while $\overline{y}$ and $\overline{z}$ correspond to the principal axes of the cross section. The y- and z-axes are parallel to the principal ones but having their origin at the shear center, i.e. the point **C**. Besides a circumferential co-ordinate system $\{\mathbf{A}:x,s,n\}$ is defined in the middle contour of the cross-section. On the other hand, y_0 and z_0 are the centroidal co-ordinates measured with respect to the shear center.

The mathematical model for the structure is based on the following hypotheses [19,21]:

(a) The cross-section contour is rigid in its own plane.
(b) Shell force and shell moment corresponding to the circumferential stress σ_{ss} and shell shear forces corresponding to the in-thickness stresses σ_{ns} and σ_{xn} are neglected.
(c) The radius of curvature at any point of the shell is neglected.
(d) Twisting curvature of the shell is expressed according to the classical plate theory, but bending curvature is expressed according to the first order shear deformation theory; in fact, bending shear strain of the wall is incorporated.

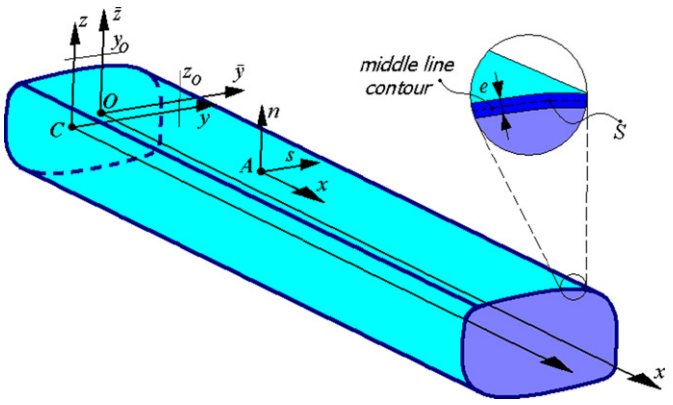

Fig. 1. Beam configuration.

(e) The strains are considered small and the rotations are considered moderate.

In order to construct the model for thin-walled beams with functionally graded properties the following hypothesis are incorporated:

(f) The properties are graded along the wall-thickness e according to a prescribed law that is uniform around the contour domain S and depends only on the thickness variable n.
(g) Shear effects across the wall-thickness e are neglected.
(h) The temperature of the beam is defined in a prescribed steady state and it is assumed to vary only along the thickness of the cross-section.

The variation laws of the material properties along the wall thickness can be prescribed in order to bear in mind with different types of material gradation such as metal to ceramic or metal to metal (e.g. steel and aluminium). Functionally graded shells are usually considered to be composed of many isotropic homogeneous layers [23]. Thus, the stress–strain relations for a generally isotropic material including thermal effects are expressed as [12,24]

$$\begin{Bmatrix}\sigma_{xx}\\ \sigma_{ss}\\ \sigma_{xn}\\ \sigma_{ns}\\ \sigma_{xs}\end{Bmatrix}=\begin{bmatrix}Q_{11} & Q_{12} & 0 & 0 & 0\\ Q_{12} & Q_{11} & 0 & 0 & 0\\ 0 & 0 & Q_{44} & 0 & 0\\ 0 & 0 & 0 & Q_{55} & 0\\ 0 & 0 & 0 & 0 & Q_{66}\end{bmatrix}\begin{Bmatrix}\varepsilon_{xx}\\ \varepsilon_{ss}\\ \varepsilon_{xn}\\ \varepsilon_{ns}\\ \varepsilon_{xs}\end{Bmatrix}-\begin{Bmatrix}\overline{Q}_{11}\alpha_f\Delta T\\ \overline{Q}_{11}\alpha_f\Delta T\\ 0\\ 0\\ 0\end{Bmatrix}. \tag{1}$$

The elements Q_{ij} are defined in terms of the following effective elastic properties:

$$Q_{11}=\frac{E_f}{1-v_f^2},\quad Q_{12}=\frac{E_f v_f}{1-v_f^2},\quad \overline{Q}_{11}=\frac{E_f}{1-v_f},$$

$$Q_{44}=Q_{55}=Q_{66}=\frac{E_f}{2(1+v_f)}. \tag{2}$$

The material properties can vary according to the following power law:

$$E_f(n)=(E_o-E_i)\left(\frac{n}{e}+\frac{1}{2}\right)^K+E_i, \tag{3}$$

$$v_f(n)=(v_o-v_i)\left(\frac{n}{e}+\frac{1}{2}\right)^K+v_i, \tag{4}$$

$$\alpha_f(n)=(\alpha_o-\alpha_i)\left(\frac{n}{e}+\frac{1}{2}\right)^K+\alpha_i, \tag{5}$$

$$\rho_f(n)=(\rho_o-\rho_i)\left(\frac{n}{e}+\frac{1}{2}\right)^K+\rho_i, \tag{6}$$

$$\kappa_f(n)=(\kappa_o-\kappa_i)\left(\frac{n}{e}+\frac{1}{2}\right)^K+\kappa_i, \tag{7}$$

in which E_f, v_f, α_f, ρ_f and κ_f are the graded modulus of elasticity, Poisson's coefficient, thermal expansion coefficient, mass density and thermal conductivity coefficient, respectively. These properties are defined in $n\in[-e/2,e/2]$, where e is the thickness. The subindexes 'o' and 'i' stand for outer and inner surfaces, respectively. $K(0\le K\le\infty)$ is the power law exponent. It becomes evident that if $K=0$ the beam is entirely made of the outer material, normally ceramic. Fig. 2 shows an example of properties variation across the thickness for different values of the exponent K. In addition to the power laws of variation in the radial direction, the properties may be subjected to variation with the temperature that can be represented

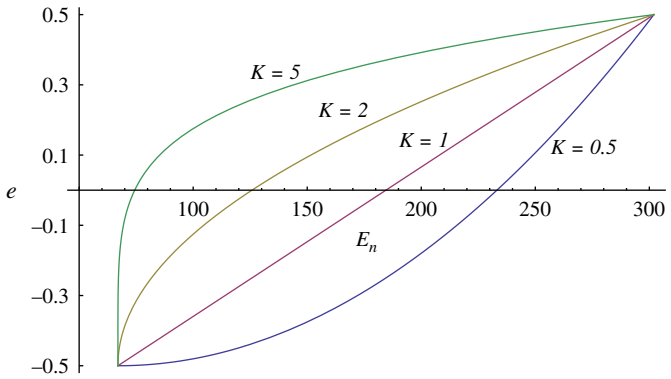

Fig. 2. Example of properties varying across the thickness.

by the following expression [1,11]:

$$m_p=m_{p0}(c_0T^{-1}+1+c_1T+c_2T^2+c_3T^3), \tag{8}$$

in which m_p means a temperature-varying material property in general (i.e. modulus of elasticity E_f, or Poisson's coefficient v_f, etc.), T is the absolute temperature (°C) and the coefficients c_i and m_{p0} are unique for a particular material. These coefficients can be calculated by means of curve fitting procedures of the experimental data. Thus the material properties can be represented as a function of the thickness and the temperature. It is clear that m_{p0} is the typical material property free of thermal effects.

The temperature distribution along the thickness can be calculated through the following heat-conduction differential equation:

$$\frac{d\kappa}{dn}\frac{dT}{dn}+\kappa\frac{d^2T}{dn^2}=0,\quad T|_{n=-e/2}=T_i,\quad T|_{n=e/2}=T_o \tag{9}$$

whose solution can be deduced [25] in terms of the following series:

$$T(n)=T_i-\frac{(T_o-T_i)}{\mathcal{D}}\sum_{j=0}^{\mathcal{Z}}\frac{(-1)^j(\kappa_o-\kappa_i)^j}{(1+jK)\kappa_i^j}\left(\frac{n}{e}+\frac{1}{2}\right)^{(1+jK)},$$

$$\text{with}\quad \mathcal{D}=\sum_{j=0}^{\mathcal{Z}}\frac{(-1)^j(\kappa_o-\kappa_i)^j}{(1+jK)\kappa_i^j}, \tag{10}$$

where, the upper limit of the summation is such that $\mathcal{Z}\to\infty$, however by means of an elemental numerical study it can be proved that Eq. (10) may be finely approximated by taking just a few terms, or more practically, $\mathcal{Z}\ge 5$ as it was done by many researchers [25,26].

2.2. Motion equations and constitutive equations

The non-linear motion equations of thin-walled beams allowing for full shear deformability can be written in the following form [18]:

$$\begin{aligned}
&Q_x'+\mathcal{M}_1(x)=0,\\
&-Q_y'-\underline{(Q_xv')'}+\mathcal{M}_2(x)=0,\\
&M_z'-Q_y-\underline{Q_xz_0\phi_x'}+\mathcal{M}_3(x)=0,\\
&-Q_z'-\underline{(Q_xw')'}+\mathcal{M}_4(x)=0,\\
&M_y'-Q_z+\underline{Q_xy_0\phi_x'}+\mathcal{M}_5(x)=0,\\
&-(T_w'+T_{sv}')-\underline{(B_w\phi_x')'+Q_x(z_0\theta_z'-y_0\theta_y')}+\mathcal{M}_6(x)=0,\\
&-B'+T_w+\mathcal{M}_7(x)=0,
\end{aligned} \tag{11}$$

and subjected to the following boundary conditions (at $x=0$, and $x=L$):

$$Q_x-\overline{Q}_x=0 \quad \text{or} \quad \delta u=0,$$

$$Q_y+Q_x v'=0 \quad \text{or} \quad \delta v=0,$$

$$-M_z+(Q_x-\overline{Q}_x)z_0\phi_x=0 \quad \text{or} \quad \delta\theta_z=0,$$

$$Q_z+Q_x w'=0 \quad \text{or} \quad \delta w=0,$$

$$-M_y-(Q_x-\overline{Q}_x)y_0\phi_x=0 \quad \text{or} \quad \delta\theta_y=0,$$

$$T_w+T_{sv}+B_w\phi_x'-\overline{Q}_x(z_0\theta_z-y_0\theta_y)=0 \quad \text{or} \quad \delta\phi_x=0,$$

$$B=0 \quad \text{or} \quad \delta\theta_x=0. \tag{12}$$

In Eqs. (11) and (12) primes mean derivation with respect to the space variable x. The underlined terms correspond to non-linear coupling between the axial dynamic forces and the lateral and twisting motions. Depending on the hypotheses invoked some of those underlined terms can be neglected, as it will shown further in the present work for illustrative purposes. The variable u is the axial displacement of the cross-section, v and w are the lateral displacements of the shear center, θ_y and θ_z are bending rotation parameters, ϕ_x is the twisting angle measured from the shear center and θ_x is a measure of the warping intensity. On the other hand, Q_x is the axial force, Q_y and Q_z are shear forces, M_y and M_z are bending moments, B is the bimoment, T_{sv} is the twisting moment due to pure torsion and T_w is the flexural-torsional moment due to warping torsion. B_w is a higher-order stress-resultant related to warping torsion. $\overline{Q}_x$ is the prescribed axial force acting at the boundaries. Finally, $\mathcal{M}_j(x)$, $j=1,\ldots,7$ are the inertia forces. These inertia forces can be expressed in terms of the accelerations as follows:

$$\begin{Bmatrix}\mathcal{M}_1\\ \mathcal{M}_2\\ \mathcal{M}_3\\ \mathcal{M}_4\\ \mathcal{M}_5\\ \mathcal{M}_6\\ \mathcal{M}_7\end{Bmatrix}=\begin{bmatrix} J_{11}^{\rho} & 0 & 0 & 0 & 0 & 0 & 0\\ & J_{11}^{\rho} & 0 & 0 & 0 & -z_0J_{11}^{\rho} & 0\\ & & J_{22}^{\rho} & 0 & 0 & 0 & 0\\ & & & J_{11}^{\rho} & 0 & y_0J_{11}^{\rho} & 0\\ & & & & J_{33}^{\rho} & 0 & 0\\ & Sym & & & & J_{00}^{\rho} & 0\\ & & & & & & J_{44}^{\rho}\end{bmatrix}\begin{Bmatrix}\ddot{u}\\ \ddot{v}\\ \ddot{\theta}_z\\ \ddot{w}\\ \ddot{\theta}_y\\ \ddot{\phi}_x\\ \ddot{\theta}_x\end{Bmatrix}. \tag{13}$$

The dots over the variables intend for derivation with respect to the time, that is $(\dot{\bullet})=d(\bullet)/dt$. The inertia coefficients J_{ij}^{ρ} are such that:

$$J_{ij}^{\rho}=\int_A\rho(n)\overline{g}_i\overline{g}_j\,ds\,dn, \quad \text{with } \overline{g}=\left\{1,\overline{Y}-n\frac{dZ}{ds},\overline{Z}+n\frac{dY}{ds},\omega_p(s)-nl(s)\right\},$$

$$J_{00}^{\rho}=\int_A\rho(n)(Y^2+Z^2)\,ds\,dn. \tag{14}$$

The beam forces involved in Eq. (11) can be defined in terms of the shell stress-resultants according to

$$Q_x=\int_S N_{xx}\,ds, \quad B=\int_S[N_{xx}\omega_p-M_{xx}l(s)]\,ds,$$

$$Q_y=\int_S\left(N_{xs}\frac{dY}{ds}\right)ds, \quad Q_z=\int_S\left(N_{xs}\frac{dZ}{ds}\right)ds,$$

$$M_y=\int_S\left(N_{xx}\overline{Z}+M_{xx}\frac{dY}{ds}\right)ds, \quad M_z=\int_S\left(N_{xx}\overline{Y}-M_{xx}\frac{dZ}{ds}\right)ds,$$

$$T_w=\int_S[N_{xs}(r(s)-\psi)]\,ds, \quad T_{sv}=\int_S(N_{xs}\psi-2M_{xs})\,ds,$$

$$B_w=\int_S[N_{xx}(Y^2+Z^2)-2M_{xx}r(s)]\,ds, \tag{15}$$

where ω_p is the contour warping function, ψ is the shear strain at the middle line, obtained by means of the Saint-Venant theory of pure torsion for isotropic beams, and normalized with respect to twisting angle gradient [19,21,27]. $\{Y,Z\}$ and $\{\overline{Y},\overline{Z}\}$ are the co-ordinates corresponding to points lying on the middle line of the cross-sectional wall, measured from the shear center and the centroid, respectively. The functions $r(s)$ and $l(s)$ are defined as follows:

$$r(s)=-Z(s)\frac{dY}{ds}+Y(s)\frac{dZ}{ds}, \quad l(s)=Y(s)\frac{dY}{ds}+Z(s)\frac{dZ}{ds}. \tag{16}$$

From the conventional definitions of shell stress-resultants given by

$$N_{xx}=\int_{-e/2}^{e/2}\sigma_{xx}\,dn, \quad N_{ss}=\int_{-e/2}^{e/2}\sigma_{ss}\,dn, \quad N_{xs}=\int_{-e/2}^{e/2}\sigma_{xs}\,dn,$$

$$M_{xx}=\int_{-e/2}^{e/2}\sigma_{xx}n\,dn, \quad M_{ss}=\int_{-e/2}^{e/2}\sigma_{ss}n\,dn, \quad M_{xs}=\int_{-e/2}^{e/2}\sigma_{xs}n\,dn, \tag{17}$$

substituting Eq. (1) into Eq. (17), taking into account hypotheses (b), (e), and (g), and assuming that $N_{ss}=M_{ss}=0$, after an algebraic rearrangement it is possible to derive [22] the following constitutive equation of shell-forces accounting for thermal effects:

$$\begin{Bmatrix}N_{xx}\\ N_{xs}\\ M_{xx}\\ M_{xs}\end{Bmatrix}=\begin{bmatrix}\overline{A}_{11} & 0 & \overline{B}_{11} & 0\\ 0 & \overline{A}_{66} & 0 & \overline{B}_{66}\\ \overline{B}_{11} & 0 & \overline{D}_{11} & 0\\ 0 & \overline{B}_{66} & 0 & \overline{D}_{66}\end{bmatrix}\begin{Bmatrix}\mu_{xx}\\ \mu_{xs}\\ \chi_{xx}\\ \chi_{xs}\end{Bmatrix}-\begin{bmatrix}\overline{T}_{NN} & 0 & \overline{T}_{NM} & 0\\ 0 & 0 & 0 & 0\\ \overline{T}_{MN} & 0 & \overline{T}_{MM} & 0\\ 0 & 0 & 0 & 0\end{bmatrix}\begin{Bmatrix}Q_N^{(T)}\\ 0\\ Q_M^{(T)}\\ 0\end{Bmatrix}, \tag{18}$$

where μ_{xx} and μ_{xs} are longitudinal and tangential shell strains, respectively, χ_{xx} and χ_{xs} are the corresponding curvatures, whereas $Q_N^{(T)}$ and $Q_M^{(T)}$ are defined according to

$$\begin{Bmatrix}Q_N^{(T)}\\ Q_M^{(T)}\end{Bmatrix}=\int_{-e/2}^{e/2}\overline{Q}_{11}\alpha_f\Delta T\begin{Bmatrix}1\\ n\end{Bmatrix}dn. \tag{19}$$

Definitions of elastic coefficients $\overline{A}_{ij}$, $\overline{B}_{ij}$, $\overline{D}_{ij}$ and thermal expansion coefficients employed in Eq. (18) may be followed in Appendix A.

The shell strains μ_{xx}, μ_{xs}, χ_{xx} and χ_{xs} can be expressed in the following form [18]:

$$\mu_{xx}=\varepsilon_{D1}+\overline{Z}\varepsilon_{D2}+\overline{Y}\varepsilon_{D3}+\omega_p\varepsilon_{D4}+(Y^2+Z^2)\varepsilon_{D9},$$

$$\mu_{xs}=\frac{dY}{ds}\varepsilon_{D5}+\frac{dZ}{ds}\varepsilon_{D6}+(r(s)-\psi)\varepsilon_{D7}+\psi\varepsilon_{D8},$$

$$\chi_{xx}=\frac{dY}{ds}\varepsilon_{D2}-\frac{dZ}{ds}\varepsilon_{D3}-l(s)\varepsilon_{D4}-2r(s)\varepsilon_{D9},$$

$$\chi_{xs}=-2\varepsilon_{D8}, \tag{20}$$

where the generalized strains ε_{Dj}, $j=1,\ldots,9$ are given as follows [18]:

$$\varepsilon_{D1}=u'+\tfrac{1}{2}(v'^2+w'^2)+\phi_x(z_0\theta_z'-y_0\theta_y'),$$

$$\varepsilon_{D2}=-\theta_y'+\theta'_z\phi_x, \quad \varepsilon_{D3}=-\theta_z'-\theta'_y\phi_x,$$

$$\varepsilon_{D4}=\theta_x'-\frac{1}{2}(\theta_z\theta_y''-\theta_y\theta_z''), \quad \varepsilon_{D5}=(v'-\theta_z)-\frac{z_0}{2}(\theta_z\theta_y'-\theta_y\theta_z'),$$

$$\varepsilon_{D6}=(w'-\theta_z)+\frac{y_0}{2}(\theta_z\theta_y'-\theta_y\theta_z'), \quad \varepsilon_{D7}=\phi_x'-\theta_x,$$

$$\varepsilon_{D8}=\phi_x'-\frac{1}{2}(\theta_z\theta_y'-\theta_y\theta_z'), \quad \varepsilon_{D9}=\frac{\phi_x'^2}{2}. \tag{21}$$

Now taking into account the definition of the beam forces given in Eq. (15) and employing the definitions of shell forces and strains

given in Eqs. (18) and (20) one gets the following expression of the generalized beam forces as

$$\mathbf{F} = \mathbf{J}_E \Delta - \mathbf{J}_T \mathbf{Q}_T, \tag{22}$$

where $\mathbf{F}$, Δ and $\mathbf{Q}_T$ are defined as

$$\mathbf{F} = \{Q_x \;\; M_y \;\; M_z \;\; B \;\; Q_y \;\; Q_z \;\; T_w \;\; T_{sv} \;\; B_w\}^T,$$

$$\Delta = \{\varepsilon_{D1} \;\; \varepsilon_{D2} \;\; \varepsilon_{D3} \;\; \varepsilon_{D4} \;\; \varepsilon_{D5} \;\; \varepsilon_{D6} \;\; \varepsilon_{D7} \;\; \varepsilon_{D8} \;\; \varepsilon_{D9}\}^T,$$

$$\mathbf{Q}_T = \{Q_N^{(T)} \;\; 0 \;\; Q_M^{(T)} \;\; 0\}^T. \tag{23}$$

The matrix $\mathbf{J}_E$ of stiffness coefficients and the matrix $\mathbf{J}_T$ of thermal-coupled rigidity coefficients are given by

$$\mathbf{J}_E = \int_S \mathbf{M}_D^T \mathbf{N}_E \mathbf{M}_D \, ds, \quad \mathbf{J}_T = \int_S \mathbf{M}_D^T \mathbf{N}_T \, ds, \tag{24}$$

where $\mathbf{N}_E$, $\mathbf{N}_T$ and $\mathbf{M}_D$ are defined as follows:

$$\mathbf{N}_E = \begin{bmatrix} \overline{A}_{11} & 0 & \overline{B}_{11} & 0 \\ 0 & \overline{A}_{66} & 0 & \overline{B}_{66} \\ \overline{B}_{11} & 0 & \overline{D}_{11} & 0 \\ 0 & \overline{B}_{66} & 0 & \overline{D}_{66} \end{bmatrix}, \quad \mathbf{N}_T = \begin{bmatrix} \overline{T}_{NN} & 0 & \overline{T}_{NM} & 0 \\ 0 & 0 & 0 & 0 \\ \overline{T}_{MN} & 0 & \overline{T}_{MM} & 0 \\ 0 & 0 & 0 & 0 \end{bmatrix}, \tag{25}$$

$$\mathbf{M}_D = \begin{bmatrix} 1 & \overline{Z} & \overline{Y} & \omega_p & 0 & 0 & 0 & 0 & Y^2+Z^2 \\ 0 & 0 & 0 & 0 & dY/ds & dZ/ds & r(s)-\psi & \psi & 0 \\ 0 & dY/ds & -dZ/ds & -l(s) & 0 & 0 & 0 & 0 & -2r(s) \\ 0 & 0 & 0 & 0 & 0 & 0 & 0 & -2 & 0 \end{bmatrix}. \tag{26}$$

Final remarks should be mentioned in order to clarify some features of the present model. As it was mentioned before Eq. (11) has been derived invoking a set of hypotheses. However, as a consequence of the hypotheses formulated in the displacement field, such as incorporation or not of second order rotational terms (see [18,21]), some important terms may disappear in the algebraic process. This aspect is important because it may lead to inappropriate motion equations and consequently to inaccurate predictions of the dynamic behavior of thin-walled beams in general. Thus, in a formulation incorporating only first order rotational terms, all simply underlined terms of Eq. (11) are eliminated.

3. Dynamic stability

3.1. Basic description

In this section the dynamic stability of a simply supported thin-walled FGM beam is analyzed considering an axial excitation given by the following expression:

$$P(t) = P_o + P_d \cos[\varpi t], \tag{27}$$

where ϖ is the excitation frequency, $P_o = \alpha P_{cr}$, $P_d = \beta P_{cr}$, α is the static load factor, β is the dynamic load factor and P_{cr} is the critical load of the beam. When the beam is excited in the axial (longitudinal) direction, and the interaction of this movement on the other motions has to be studied, the coupling of these various motions depends on the symmetry of the cross-section analyzed. The first differential equation shown in Eq. (11), corresponding to the longitudinal movement can be easily solved, disregarding longitudinal inertia forces, in the following form:

$$Q_x = -P_o - P_d \cos[\varpi t]. \tag{28}$$

Longitudinal inertia forces can substantially affect the dynamic stability of a beam when the excitation frequency of Q_x is near the longitudinal natural frequencies of the beam, i.e., when the longitudinal vibrations have a resonant character. However, in this section and only for comparative purposes, the solution procedure is developed disregarding longitudinal inertia forces. The effect of longitudinal inertia forces is afterwards accounted for once the expressions of the previous solution are attained. The remaining differential equations can be discretized by means of the following wave functions:

$$v = v_o(t)\sin[\lambda_k x], \quad w = w_o(t)\sin[\lambda_k x], \quad \phi_x = \phi_{xo}(t)\sin[\lambda_k x],$$

$$\theta_z = \theta_{zo}(t)\cos[\lambda_k x], \quad \theta_y = \theta_{yo}(t)\cos[\lambda_k x], \quad \theta_x = \theta_{xo}(t)\cos[\lambda_k x], \tag{29}$$

where $v_o(t)$, $w_o(t)$, $\phi_{xo}(t)$, $\theta_{yo}(t)$, $\theta_{zo}(t)$ and $\theta_{xo}(t)$ are the associated displacement amplitudes which are time dependent. On the other hand, the wave number is defined as

$$\lambda_k = \frac{k\pi}{L}, \quad k = 1,2,3,\ldots \tag{30}$$

The substitution of Eqs. (28) and (29) into the last six equations of Eq. (11) leads to a system of ordinary differential equations, which can be expressed in a compact form, by using matrix notations, as

$$\mathbf{M}\ddot{\mathbf{U}} + (\mathbf{K} - P(t)\mathbf{S})\mathbf{U} = \mathbf{O}, \tag{31}$$

where

$$\mathbf{U} = \{v_o, \theta_{zo}, w_o, \theta_{yo}, \phi_{xo}, \theta_{xo}\}^T, \tag{32}$$

$$\mathbf{M} = \begin{bmatrix} J_{11}^\rho & 0 & 0 & 0 & -z_o J_{11}^\rho & 0 \\ & J_{22}^\rho & 0 & 0 & 0 & 0 \\ & & J_{11}^\rho & 0 & y_o J_{11}^\rho & 0 \\ & & & J_{33}^\rho & 0 & 0 \\ & sym & & & J_{00}^\rho & 0 \\ & & & & & J_{11}^\rho \end{bmatrix}, \tag{33}$$

$$\mathbf{S} = \begin{bmatrix} \lambda_k^2 & 0 & 0 & 0 & -z_o\lambda_k & 0 \\ & 0 & 0 & 0 & 0 & 0 \\ & & \lambda_k^2 & 0 & y_o\lambda_k & 0 \\ & & & 0 & 0 & 0 \\ & sym & & & \lambda_k^2 J_{19}^E / J_{11}^E & 0 \\ & & & & & 0 \end{bmatrix}, \tag{34}$$

$$\mathbf{K} = \begin{bmatrix} J_{55}\lambda_k^2 & -J_{55}\lambda_k & J_{56}\lambda_k^2 & -J_{56}\lambda_k & J_{57}\lambda_k^2 & -J_{57}\lambda_k \\ & J_{33}\lambda_k^2 + J_{55} & -J_{56}\lambda_k & J_{56} & -J_{57}\lambda_k & J_{57} \\ & & J_{66}\lambda_k^2 & -J_{66}\lambda_k & J_{67}\lambda_k^2 & -J_{67}\lambda_k \\ & & & J_{22}\lambda_k^2 + J_{66} & -J_{67}\lambda_k & J_{67} \\ & sym & & & (J_{88}+J_{77})\lambda_k^2 & -J_{77}\lambda_k^2 \\ & & & & & J_{44}\lambda_k^2 - J_{77} \end{bmatrix}, \tag{35}$$

$\mathbf{M}$, $\mathbf{S}$ and $\mathbf{K}$ are the mass matrix, geometric stiffness matrix and elastic stiffness matrix, respectively. The stiffness coefficients J_{ij} are calculated with Eq. (24).

Now, from Eq. (31) one can obtain the solution to different problems. Then, the problem concerning determination of free vibration frequencies of a beam loaded by a constant longitudinal force can be expressed as

$$|\mathbf{K} - P_o\mathbf{S} - \Omega^2\mathbf{M}| = 0. \tag{36}$$

The problem of determination of free vibration frequencies of an unloaded beam leads to the following equation:

$$|\mathbf{K} - \Omega^2\mathbf{M}| = 0. \tag{37}$$

Finally, the buckling problem can be analyzed from the following equation:

$$|\mathbf{K}-P_o\mathbf{S}|=0. \tag{38}$$

3.2. Principal parametric resonance

The regions of parametric resonance of thin-walled beams subjected to an axial periodic load are studied in this section. In the classification of parametric resonance, if ϖ is the excitation frequency and Ω_i the natural frequency of the ith mode, parametric resonance of "first kind" is said to occur when $\varpi/(2\Omega)\approx 1/r$, $r=1,2,\ldots$, while parametric resonance of the "second kind" is said to occur when $\varpi/(\Omega_k+\Omega_j)\approx 1/r$, $r=1,2,\ldots,(k\neq j)$. In both cases the situation where $r=1$ is of the most practical importance. Usually the parametric resonance of the first kind is termed "parametric resonance", whereas the second kind is referred as "combination resonance", because it involves two different frequencies. In this paper the study is only focused on the case of parametric resonance.

The problem of finding the boundaries of the stability regions, simply leads to the determination of the conditions under which Eq. (31) has periodic solutions with period $2\pi/\varpi$ and $4\pi/\varpi$ [16]. In the case of the principal region, which is half sub-harmonic, a solution is looked for with a periodical function whose period is twice the excitation frequency: i.e., $4\pi/\varpi$. The condition for the existence of solutions can be expressed in the following infinite determinant form [16]:

$$\begin{vmatrix} \mathbf{K}-\mathbf{S}(P_o\pm\frac{1}{2}P_d)-\frac{1}{4}\varpi^2\mathbf{M} & -\frac{1}{2}P_d\mathbf{S} & 0 & \cdots \\ & \mathbf{K}-P_o\mathbf{S}-\frac{9}{4}\varpi^2\mathbf{M} & -\frac{1}{2}P_d\mathbf{S} & \cdots \\ sym & & \mathbf{K}-P_o\mathbf{S}-\frac{25}{\varpi}^2\mathbf{M} & \cdots \\ \cdots & \cdots & \cdots & \cdots \end{vmatrix}=0. \tag{39}$$

The boundaries of the stability regions lying near the frequency $\varpi=2\Omega$ can be determined with sufficient accuracy considering only the first leading diagonal term, i.e.

$$|\mathbf{K}-\mathbf{S}(P_o\pm\tfrac{1}{2}P_d)-\tfrac{1}{4}\varpi^2\mathbf{M}|=0. \tag{40}$$

3.3. Influence of forced and parametrically excited vibrations

In the previous sections the longitudinal internal force acting along the beam is assumed equal to the external force acting at the ends of the beam, then longitudinal vibrations are neglected. Such an assumption is acceptable for certain bounds where the excitation frequency is small in comparison with the frequency ω_L, i.e. the one corresponding to free longitudinal vibrations. However, for beams with small slenderness ratio or particular distribution of material properties, the frequency at which a parametric resonance occurs, can be of the same order of the natural frequency of the longitudinal vibrations. In this context, with the objective to include this effect in the analysis, it is necessary to substitute the constitutive expression of the axial force Q_x into the first differential equation in Eq. (11) and integrating it in terms of the displacement u, that is

$$-J_{11}\frac{\partial^2 u}{\partial x^2}+J_{11}^{\rho}\frac{\partial^2 u}{\partial t^2}=0. \tag{41}$$

Adopting the appropriate boundary condition, i.e. the first of Eq. (12), the solution to the Eq. (41) can be represented as

$$u(x,t)=\frac{P_o x}{J_{11}}+\frac{P_d\sin[\eta x]}{\eta J_{11}\cos[\eta L]}\cos[\varpi t], \tag{42}$$

where

$$\eta=\varpi\sqrt{\frac{J_{11}^{\rho}}{J_{11}}} \tag{43}$$

Substituting Eq. (42) into the remaining six differential equations given in Eq. (11) and applying the same methodology previously explained, Eq. (40) can be expressed in the following compact form:

$$\left|\mathbf{K}-\mathbf{S}\left(P_o\pm\frac{1}{2}P_d\frac{\tan[\eta L]}{\eta L}\right)-\frac{1}{4}\varpi^2\mathbf{M}\right|=0. \tag{44}$$

Now, solving Eq. (44) leads to the main regions of stability considering the influence of the longitudinal vibration.

4. Applications and numerical results

In this section, the aforementioned model is employed in order to study the dynamic stability of simply supported thin-walled beams with graded properties. The influence of longitudinal vibrations and the effect of shear deformation on the regions of stability is analyzed. When the beam is excited in the axial (longitudinal) direction, the interaction of this movement will depend on the symmetry of the cross-section analyzed. Different bisymmetrical cross-sectional shapes and beam lengths are considered to perform the numerical analysis. The effect of variation of the volume fraction of ceramic/metallic components is evaluated. This may be done by means of the exponent K. The first set of examples is carried out disregarding temperature effects. The elastic and mass properties of the material constituents (Steel, Alumina, Aluminium and Silicon Carbide) are summarized in Table 1.

In the following examples (associated with the cross-sections shown in Fig. 3), because of the by-symmetry ($y_0=z_0=0$), the motion equations are uncoupled. Therefore, there are three main modes of vibration corresponding either to bending, in y-direction and z-direction, or to torsion. In these cases, the lowest frequency corresponds to the lateral bending mode (y-direction), while the highest vibration frequency corresponds to the twist mode. In all of the following cases, the value of the static load parameter was $\alpha=0.5$, and the excitation frequency ϖ was scaled with the lowest value of parametric resonance frequency (i.e. the case when the frequency related to the first mode is doubled, or formally $\varpi=2\Omega_1$).

Table 1
Properties of Steel, Alumina (Al_2O_3), Aluminium (Al) and Silicon Carbide (SiC) at $T=300$ °C.

Properties	Steel	Al_2O_3	Al	SiC
E (Pa)	206×10^9	393×10^9	67×10^9	302×10^9
ν	0.30	0.25	0.33	0.17
ρ (kg m^{-3})	7800	3960	2700	3200

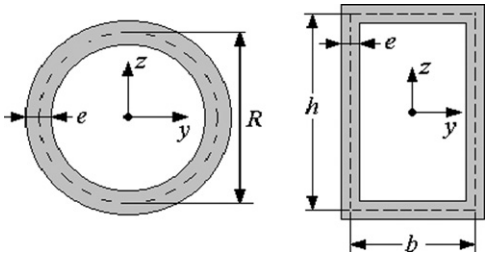

Fig. 3. Cross-sectional cases and their dimensions.

4.1. Instability regions for different gradation intensity

The first example consists of a box-beam with the following geometrical properties: $L=0.2$ m, $h/L=0.05$, $b/h=0.5$ and $e/h=0.15$. The material properties are graded from an inner surface of aluminium to an outer surface of Silicon Carbide. The first two stability regions associated with bending vibration modes are shown in Fig. 4. In this figure different cases of gradation properties (i.e. changing the exponent K) are depicted. The excitation frequency ϖ is scaled with the lowest frequency value of parametric resonance corresponding to $K=10$. The natural frequencies (measured in (Hz)) are shown in Table 2, considering the dynamic load parameter $\beta=0$. The frequency referred to the unloaded beam ($\alpha=0$) is denoted by ω and, on the other hand Ω is the natural frequency of the beam when it is subjected to a static load ($\alpha=0.5$). It may be observed that the widest unstable region corresponds to the first mode (or to the main frequency of parametric resonance), while the smallest region is associated with the second mode (or second frequency of parametric resonance). The width of the unstable regions grows with decreasing values of the exponent K. The parametric regions associated to torsional modes are quite narrow and located far away from the main unstable region. Moreover, the influence of the longitudinal inertia is negligible in all the cases analyzed, because the excitation frequency is small in comparison to the free longitudinal vibration frequency ω_L. This behavior can be observed from the frequencies shown in Table 2. It can be noted that the vibration frequencies (ω) are decreasing for a given static load parameter. This decrease is about 30% for the first bending (lateral) mode, 10% for the first bending (vertical) mode and 0.5% for the torsional mode. This effect keeps constant for the three cases of exponent K analyzed.

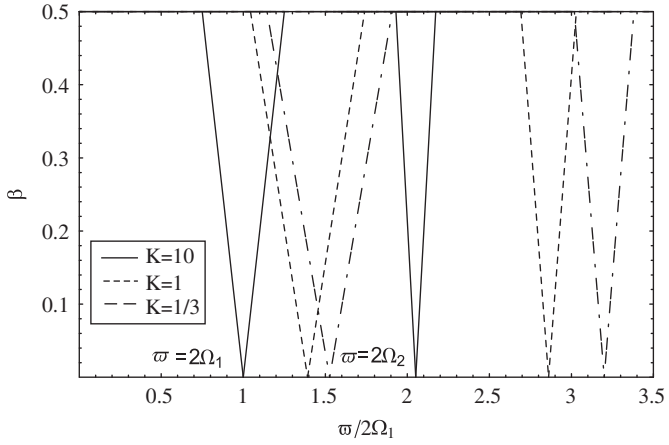

Fig. 4. Comparison of unstable regions for different values of K.

Table 2
Natural frequencies for a box beam (Hz), $L=0.2$ m.

K	Modes	ω_i	Ω_i	ω_L
10	1	521.14	368.5	7095.21
	2	840.89	756.04	
	3	7632.03	7622.76	
1	1	725.46	512.97	9885.46
	2	1172.20	1054.26	
	3	10860.40	10847.80	
1/3	1	795.38	562.42	11118.83
	2	1306.18	1179.18	
	3	11843.10	11829.60	

In Fig. 5 the variation of the vibration frequency values in function on the static load is shown for different values of the exponent K. The case corresponds to the first bending mode. The higher value of static load, when the frequency value is $\Omega=0$, is associated with the buckling load. In this case, the critical load of the beam corresponding to the bending mode can be easily obtained by means of the following expression (as explained in Ref. [19]):

$$P_{CR}=\frac{\pi^2}{L^2}\frac{J_{33}J_{55}}{J_{55}+J_{33}\frac{\pi^2}{L^2}}. \tag{45}$$

4.2. Instability regions: influence of longitudinal vibration

The second example corresponds to a box section with the following geometrical properties $L=0.5$ m, $h/L=0.1$, $b/h=0.5$ and $e/h=0.1$. The properties are graded from a metallic inner surface of aluminium to a ceramic outer surface of Silicon Carbide. The regions of dynamic stability for the first two frequencies of vibration excited parametrically (Ω_1 and Ω_2) are shown in Fig. 6. The first region corresponds to the bending mode in the lateral direction, while the second bending mode is in vertical direction. The third region that appears in the figure represents the influence of the longitudinal vibration, which in this case is near to the

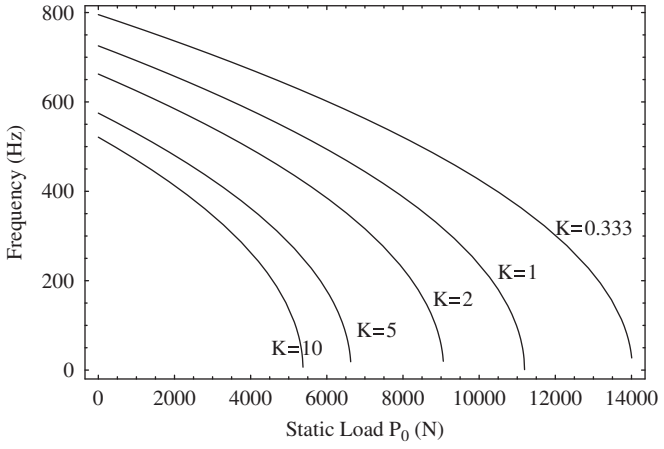

Fig. 5. Variation of frequency values versus the static load for different values of K.

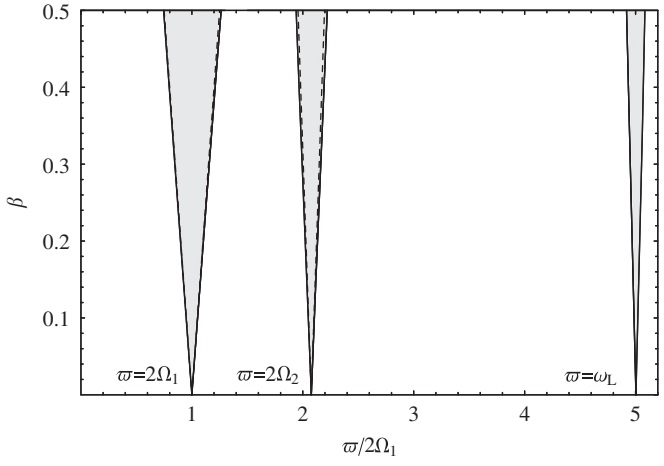

Fig. 6. Instability regions, (—) considering and (- -) neglecting longitudinal inertia, for $K=1$.

parametric unstable boundaries. Also Fig. 6 shows the unstable regions obtained by disregarding and considering the influence of the longitudinal vibration. One can observe that the size of the unstable region is nearly the same for both approaches. In this example, the influence of the volume fraction index K was considered as in the previous example. However, the dynamical behavior observed for the three cases studied ($K=10$, 1 and 1/3) was very similar, as in the previous case. Therefore, the unstable regions presented in Fig. 6 correspond to a volume fraction power index $K=1$.

The relation between the natural and the parametric excited frequency values can be observed from Table 3, considering the dynamic load parameter $\beta=0$. The variation of the frequency values in function of the static load is the same as the previous first example, where the first bending mode presents the higher decrease (about 30%).

4.3. Instability regions: influence of longitudinal vibration, more parametric analysis

In this example the influence of the longitudinal inertia is analyzed for a box section with the geometrical properties $L=0.5$ m, $h/L=0.15$, considering two different relations of $b/h=0.5$, 0.75 and $e/h=0.15$, 0.05. The material properties are graded from a metallic inner surface of aluminium to a ceramic outer surface of Silicon Carbide, and the volume fraction considered is such that $K=1$. The regions of dynamic stability for the first two frequencies of vibration excited parametrically (Ω_1 and Ω_2) are shown in Figs. 7 and 8, for $b/h=0.5$, $e/h=0.15$ and $b/h=0.75$, $e/h=0.05$, respectively. These figures show comparative results between the unstable regions obtained by considering (solid line) and disregarding (dashed line) the influence of the longitudinal vibration. It can be observed that the larger size corresponds to the main unstable region ($2\Omega_1$) in comparison with the second ($2\Omega_2$) and third unstable region (ω_L). The influence of the longitudinal inertia enlarges the unstable parametric regions. Therefore, its removal leads, inadvertently, in a less critical behavior than in the case of its incorporation. The interaction of forced and parametrically excited vibrations is more noticeable for the second cross-section analyzed (Fig. 8). This is due to the nearness of the longitudinal frequency with the parametrically excited frequency. The natural frequencies (measured in (Hz)) are shown in Table 4, for the unloaded beam $\alpha=0$ and for $\alpha=0.5$, considering the dynamic load parameter $\beta=0$.

Table 3
Natural frequencies for a box beam (Hz), $L=0.5$ m.

K	Modes	ω_i	Ω_i	ω_L
10	1	400.48	283.18	2838.08
	2	651.72	587.51	
	3	2924.39	2910.19	
1	1	558.49	394.92	3954.19
	2	909.42	819.94	
	3	4175.46	4156.13	
1/3	1	617.69	436.78	4447.23
	2	1017.09	919.35	
	3	4609.14	4588.08	

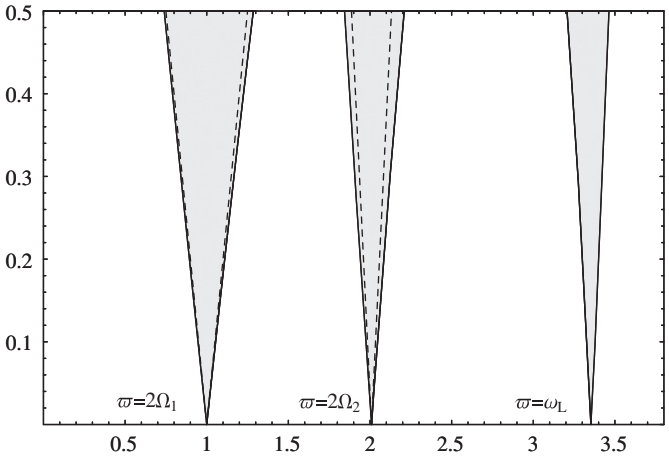

Fig. 7. Instability regions, (—) considering and (- -) neglecting longitudinal inertia, for $b/h=0.50$, $e/h=0.15$.

4.4. Instability regions: influence of shear flexibility

The influence of shear deformation on the dynamic behavior is analyzed in this example. The geometrical properties corresponding to a box beam are $L=0.5$ m, $h/L=0.15$, $b/h=0.5$ and $e/h=0.1$.

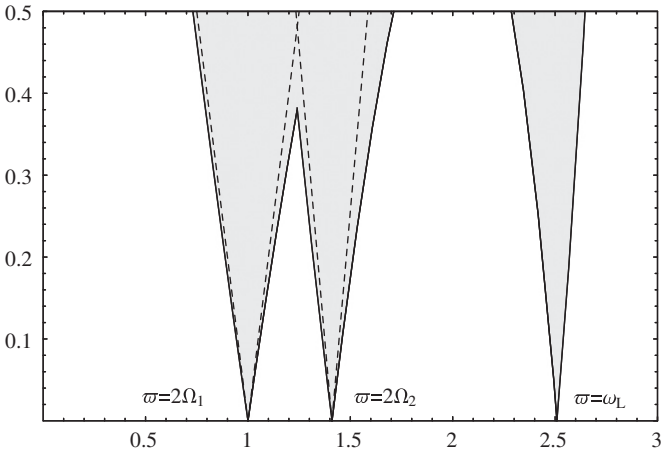

Fig. 8. Instability regions, (—) considering and (- -) neglecting longitudinal inertia, for $b/h=0.75$, $e/h=0.05$.

Table 4
Vibration frequencies for a box beam (Hz), $L=0.5$ m and $h/L=0.15$.

Ratios	Modes	ω_i	Ω_i	ω_L
$b/h=0.5$	1	834.38	590.00	3954.19
$e/h=0.15$	2	1324.43	1187.98	
	3	4346.94	4304.79	
$b/h=0.75$	1	1113.94	787.69	3954.19
$e/h=0.05$	2	1359.66	1110.63	
	3	4391.99	4318.46	

Table 5
Shear deformation effect on natural frequencies (Hz).

K	Modes	ω_i		Ω_i	
		Model I	Model II	Model I	Model II
1	1	817.06	850.96	577.75	625.20
	2	1315.75	1386.52	1184.26	1263.20
	3	4177.29	4177.34	4135.66	4135.70
1/3	1	904.75	940.19	639.75	689.43
	2	1472.88	1549.39	1329.05	1414.18
	3	4611.46	4611.53	4565.99	4566.06

The material properties are the same as the previous examples. In Table 5, natural frequencies are given considering two models: the present theory (Model I) and neglecting shear flexibility (Model II). The shear deformation in the structural model has the effect to diminish the values of the vibration frequency. The same behavior is observed for the two cases analyzed ($K=1$ and 1/3). The effect of shear flexibility on the unstable regions is shown in Fig. 9, for $K=1$. It is observed that the width of the regions does not change for both models. However, when shear deformation is neglected the unstable region moves toward the right. This is due to the increase in the parametric frequency values.

4.5. Instability regions: circular closed beam

The example considered is a circular section with the geometrical properties $L=0.2$ m, $R/L=0.15$ and $e/R=0.05$. The material properties are graded from an inner surface of steel to an outer surface of Alumina. Instability regions are shown in Fig. 10, considering a FGM such that $K=1$. The influence of the interaction between the forced vibration and the parametrically excited vibrations on the unstable regions is analyzed in such figure. The unstable boundaries obtained by disregarding the aforementioned interaction are marked in dashed lines. It is possible to observe that the widest unstable region is associated with the first and second bending modes (or in other words to the first and second frequencies of parametric resonance), while the smallest region corresponds to the torsional mode (or to the third frequency excited parametrically). In this case, the natural frequency corresponding to the longitudinal mode ω_L is next to the first parametric resonance frequency ($2\Omega_1$).

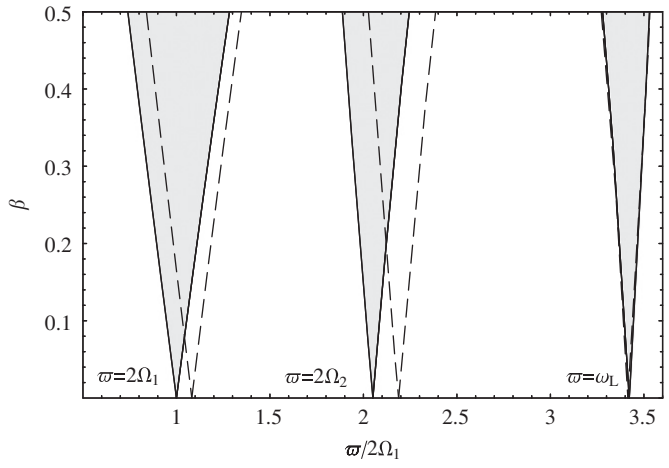

Fig. 9. Instability regions, (—) considering and (- -) neglecting shear deformation, for $K=1$.

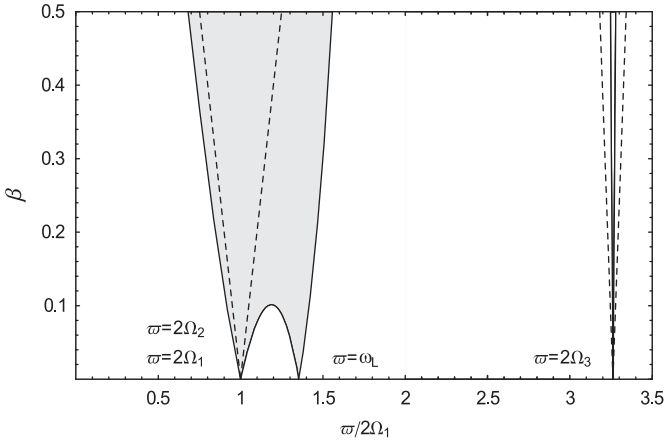

Fig. 10. Instability regions, (—) considering and (- -) neglecting longitudinal inertia, for $K=1$.

Table 6
Natural frequencies for a circular beam (Hz).

K	Modes	ω_i	Ω_i	ω_L
10	1	5693.40	4028.07	10951.4
	2	5693.40	4028.07	
	3	13656.30	13020.0	
1	1	6138.16	4342.76	11766.6
	2	6138.16	4342.76	
	3	14817.61	14135.30	
1/3	1	6337.92	4484.09	12141.45
	2	6337.92	4484.09	
	3	15327.10	14624.50	

The influence of the longitudinal inertia enlarges the first region to the right, which seems to be composed of two regions. The first unstable region ($2\Omega_1$ and $2\Omega_2$) is smaller when the interaction of the forced vibration is omitted, thus predicting a less critical behavior. However, the third unstable region ($2\Omega_3$) is larger when the interaction of the forced vibration is omitted, predicting a more conservative behavior. The interaction of forced and parametrically excited vibrations is actually the same for the three material configurations analyzed (i.e. $K=1/3$, 1 and 10). This behavior may be observed in Table 6, where natural frequencies are shown for the case of the dynamic load parameter $\beta=0$. The frequencies referred to the unloaded beam ($\alpha=0$) are denoted by ω and, on the other hand, by Ω when the beam is subjected to a static load ($\alpha=0.5$).

4.6. Instability regions: analysis of thermal effects

This example shows the influence of the thermal effects on the dynamic stability of a closed box beam constructed with a metallic alloy (Ti6Al4V) and a ceramic (ZrO_2), whose properties are given in Table 7. The geometrical properties of the box beam are $L=0.5$ m, $h/L=0.15$, $b/h=0.5$ and $e/h=0.1$. The effect of transverse temperature gradient on the unstable regions of a simply supported beam with a volume fraction exponent $K=10$ is shown in Fig. 11. In this case, the temperature of the inner metallic surface is held at a constant value of $T_m=300$ °C. The excitation frequency ϖ is scaled with the lowest frequency value of parametric resonance calculated with $\Delta T=0$ (or $T_c=300$ °C). It can be seen that the unstable region moves to the left as increase the ceramic surface temperature (T_c). As it may be expected, the parametric excited frequencies are reduced as the temperature is increases. However, in this problem type, the frequencies are not the only ones that diminish their values; the value of critical load is also affected by the gradient of temperature. The variation of frequencies and buckling load with the temperature is shown in Table 8. The natural frequency values for the beam subjected to a thermal load without mechanical static load ($\alpha=0$) are denoted by ω and for the loaded case ($\alpha=0.5$) is denoted by Ω. The influence of the temperature effect is the same in both frequencies (ω and Ω), and in this example the larger reduction is about the 15%. While in the buckling load the decrease is about 28%. The size of the unstable regions is reduced with the temperature rise and this behavior is due to the relation between the longitudinal ω_L and the parametric excited frequency Ω, see Fig. 11. The interaction of forced and parametrically excited vibrations is affected by the temperature gradient. It is observed that for large excitation load parameter β, the regions of stability

Table 7
Temperature depend coefficients of material properties for ZrO_2 and Ti6Al4V.

Properties	Material	m_{p0}	c_0	c_1	c_2	c_3
E (Pa)	Ti6Al4V	122.7×10^9	0	-4.605×10^{-4}	0	0
	ZrO_2	132.2×10^9	0	-3.805×10^{-4}	-6.127×10^{-8}	0
v	Ti6Al4V	0.2888	0	1.108×10^{-4}	0	0
	ZrO_2	0.3330	0	0	0	0
ρ (kg m^{-3})	Ti6Al4V	4420	0	0	0	0
	ZrO_2	3657	0	0	0	0
α ($^\circ$C^{-1})	Ti6Al4V	7.43×10^{-6}	0	7.483×10^{-4}	-3.621×10^{-7}	0
	ZrO_2	13.6×10^{-6}	0	-1.421×10^{-3}	9.549×10^{-7}	0
κ (W m^{-1} $^\circ$C)	Ti6Al4V	6.10	0	0	0	0
	ZrO_2	1.78	0	0	0	0

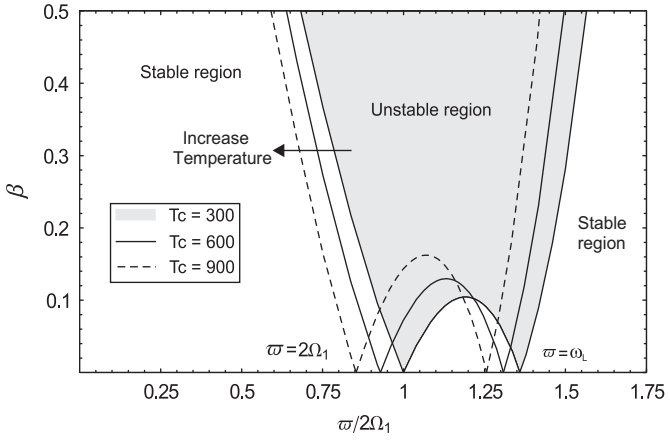

Fig. 11. Instability regions for different temperature values, with $K=10$.

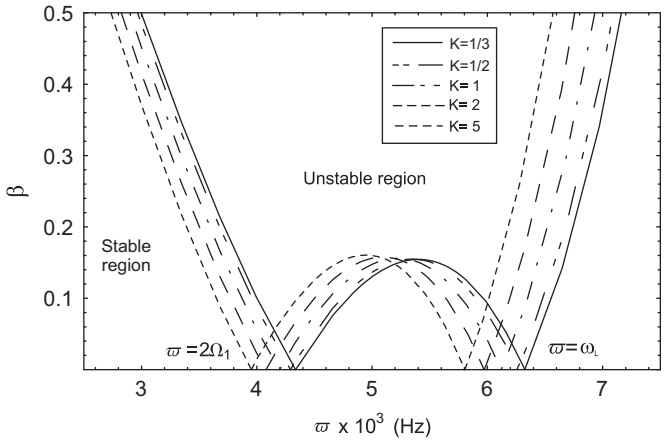

Fig. 12. Unstable boundaries for different values of volume fraction index K and $T_c=900$ °C.

Table 8
Influence of temperature on the frequency values (Hz) and buckling loads, for $T_m=300$ °C and $K=10$.

T (°C)	ω	Ω	ω_L	P_{cr} 10^6 (N)
300	3215.91	2275.25	6190.93	2.13
600	2984.39	2111.54	5961.37	1.83
900	2743.07	1940.90	5719.45	1.54

merge into one. This takes place when [16]:

$$\beta=\frac{(\omega_L^2-4\Omega^2)^2}{16\Omega^2\omega_L^2},\Rightarrow\begin{cases}\beta_{(T_c=300)}=0.098,\\ \beta_{(T_c=600)}=0.120,\\ \beta_{(T_c=900)}=0.160.\end{cases}\tag{46}$$

Fig. 12 shows the variation of the main stability regions with volume fraction exponent for a temperature gradient $\Delta T=600$ °C (i.e. temperature in the metal surface of $T_m=300$ °C and in the ceramic surface of $T_c=900$ °C). It can be seen from Table 9 that the frequency values decrease as the proportion of the ceramic volume decreases. The interaction of forced and parametrically excited vibrations is the same for the five material configurations analyzed (K). The unstable dynamic regions merge into one for the same dynamic load parameter $\beta=0.15$.

Table 9
Frequency values (Hz) and buckling loads for $T_m=300$ °C and $T_c=900$ °C.

K	ω	Ω	ω_L	P_{cr} 10^6 (N)
1/3	3064.03	2167.95	6326.02	1.71
1/2	3030.62	2144.32	6260.50	1.69
1	2959.81	2094.22	6122.38	1.67
2	2881.59	2038.88	5973.29	1.63
5	2790.75	1974.63	5805.75	1.68

5. Conclusions

The dynamic stability behavior of functionally graded thin-walled beams subjected to axial external force has been investigated considering the influence of non-conventional effects. The material properties of the functionally graded beam have been assumed to vary continuously through the thickness, according to a simple power law distribution of the volume fraction of the constituents. The formulation has been based on the context of small strains and moderate rotations theory of thin-walled beams. The dynamic stability analysis of a simply supported beam subjected to an axial periodic force system has been performed by means of Hill's method of infinite determinants developed by Bolotin. The effects of shear deformation, volume fraction index and the interaction between forced and parametrically excited vibrations on the boundaries of the unstable regions have been investigated.

From the numerical calculation carried out, it was found that regions of dynamic stability are generally wider for the first frequency of parametric resonance. Moreover, the size of the unstable regions can vary depending on the parameter K, observing that it enlarges for decreasing values of K. The effect of the

interaction between forced vibrations and the parametrically excited vibrations on the unstable regions has been observed to be considerable, when the excitation frequency is of the same order than the frequency value of the free longitudinal vibration. Moreover, the influence of the longitudinal inertia enlarges the main parametric regions. This effect keeps constant for the three material configurations analyzed. On the other hand, the shear deformation effect reduces the frequency values and this effect remains constant while the dynamical load parameter is increased. If the transverse shear is neglected an over prediction of the resonance behavior may be observed, in the sense of shifting the domain of stability toward higher excitation frequencies. On the other hand as the temperature gradient grows, the unstable region of the first parametric resonance moves to the left as a consequence of the influence of temperature in the diminution of effective material properties and the buckling loads.

Acknowledgements

The support of Universidad Tecnológica Nacional, Consejo Nacional de Investigaciones Científicas y Tecnológicas (CONICET) and ANPCYT of Argentina is kindly recognized.

Appendix A. Definition of shell coefficients

The elastic and thermoelastic coefficients introduced in Eq. (18) can be calculated with the following expressions:

$$\overline{A}_{11} = A_{11} + (2A_{12}B_{11}B_{12} - A_{11}B_{12}^2 - A_{12}^2 D_{11})/\Delta,$$

$$\overline{B}_{11} = B_{11} + (B_{11}B_{12}^2 + A_{12}B_{11}D_{12} - A_{11}B_{12}D_{12} - A_{12}B_{12}D_{11})/\Delta,$$

$$\overline{D}_{11} = D_{11} + (2D_{12}B_{11}B_{12} - A_{11}D_{12}^2 - B_{12}^2 D_{11})/\Delta,$$

$$\overline{A}_{66} = A_{66}, \quad \overline{B}_{66} = B_{66}, \quad \overline{D}_{66} = D_{66}, \tag{A.1}$$

$$\overline{T}_{NN} = 1 + (A_{12}D_{11} - B_{11}B_{12})/\Delta,$$

$$\overline{T}_{NM} = (A_{11}B_{12} - A_{12}B_{11})/\Delta,$$

$$\overline{T}_{MN} = (B_{12}D_{11} - B_{11}D_{12})/\Delta,$$

$$\overline{T}_{MM} = 1 + (A_{11}D_{12} - B_{11}B_{12})/\Delta,$$

$$\Delta = D_{11}A_{11} - B_{11}^2, \tag{A.2}$$

where

$$A_{ij} = \int_{-e/2}^{e/2} Q_{ij}\, dn, \quad B_{ij} = \int_{-e/2}^{e/2} Q_{ij} n\, dn, \quad D_{ij} = \int_{-e/2}^{e/2} Q_{ij} n^2\, dn. \tag{A.3}$$

References

[1] Reddy JN, Chin CD. Thermomechanical analysis of functionally graded cylinders and plates. Journal of Thermal Stresses 1998;26(1):593–626.
[2] Reddy JN. Analysis of functionally graded plates. International Journal of Numerical Methods in Engineering 2000;47:663–84.
[3] Praveen GN, Reddy JN. Nonlinear transient thermoelastic analysis of functionally graded ceramic-metal plates. International Journal of Solids and Structures 1998;35(33):4457–76.
[4] El-Abbasi N, Meguid SA. Finite element modeling of the thermoelastic behavior of functionally graded plates and shells. International Journal of Computational Engineering Science 2000;1(1):151–65.
[5] Kitipornchai S, Yang J, Liew KM. Semi-analytical solution for nonlinear vibration of laminated FGM plates with geometric imperfections. International Journal of Solids and Structures 2004;41(9–10):2235–57.
[6] Chakraborty A, Gopalakrishnan S, Reddy JN. A new beam finite element for the analysis of functionally graded materials. International Journal of Mechanical Sciences 2003;45:519–39.
[7] Goupee AJ, Vel SS. Optimization of natural frequencies of bidirectional functionally graded beams. Structural and Multidisciplinary Optimization 2006;32(6):473–84.
[8] Ding HJ, Huang DJ, Chen WQ. Elasticity solutions for plane anisotropic functionally graded beams. International Journal of Solids and Structures 2007;44:176–96.
[9] Xiang HJ, Yang J. Free and forced vibration of laminated FGM Timoshenko beam of variable thickness under heat conduction. Composites, Part B 2008;39:292–303.
[10] Yang J, Chen Y. Free vibration and buckling analysis of functionally graded beams with edge cracks. Composite Structures 2008;83:48–60.
[11] Oh S-Y, Librescu L, Song O. Thermoelastic modeling and vibrations of functionally graded thin-walled rotating blades. AIAA Journal 2003;41(10):2051–60.
[12] Oh S-Y, Librescu L, Song O. Vibration and instability of functionally graded circular cylindrical spinning thin-walled beams. Journal of Sound and Vibration 2005;285(4–5):1071–91.
[13] Fazelzadeh SA, Malekzadeh P, Zahedinejad P, Hosseini M. Vibration analysis of functionally graded thin-walled rotating blades under high temperature supersonic flow using the differential quadrature method. Journal of Sound and Vibration 2007;306:333–48.
[14] Fazelzadeh SA, Hosseini M. Aerothermoelastic behavior of supersonic rotating thin-walled beams made of functionally graded materials. Journal of fluids and structures 2007;23:1251–64.
[15] Nayfeh AH, Mook DT. Nonlinear oscillations. New York: Wiley and Sons; 1979.
[16] Bolotin VV. The dynamic stability of elastic systems. San Francisco: Holden-Day; 1964.
[17] Machado SP. Geometrically non-linear approximations on stability and free vibration of composite beams. Engineering Structures 2008;29(12):3567–78.
[18] Machado SP, Filipich CP, Cortínez VH. Parametric vibration of thin-walled composite beams with shear deformation. Journal of Sound and Vibration 2007;305(4–5):563–81.
[19] Machado SP, Cortínez VH. Non-linear model for stability of thin-walled composite beams with shear deformation. Thin-Walled Structures 2005;43(10):1615–45.
[20] Naj R, Sabzikar Boroujerdy M, Eslami MR. Thermal and mechanical instability of functionally graded truncated conical shells. Thin-Walled Structures 2008;46:65–78.
[21] Cortínez VH, Piovan MT. Vibration and buckling of composite thin walled beams with shear deformability. Journal of Sound and Vibration 2002;258(4):701–23.
[22] Piovan MT, Cortínez VH. Mechanics of shear deformable thin-walled beams made of composite materials. Thin-Walled Structures 2007;45:37–62.
[23] Tanigawa Y. Some basic thermoelastic problems for nonhomogeneous structural materials. Applied Mechanics Review 1995;48:287–300.
[24] Kadoli R, Ganesan N. Buckling and free vibration analysis of functionally graded cylindrical shells subjected to a temperature-specified boundary condition. Journal of Sound and Vibration 2006;289:450–80.
[25] Zhao FQ, Wang ZM, Liu HZ. Thermal post-buckling analyses of functionally graded material rod. Applied Mathematics and Mechanics 2007;28(1):59–67.
[26] Malekzadeh P. Two-dimensional in-plane free vibrations of functionally graded circular arches with temperature-dependent properties. Composite Structures 2010;91(1):38–47.
[27] Krenk S, Gunneskov O. Statics of thin-walled pre-twisted beams. International Journal of Numerical Methods in Engineering 1981;17:1407–26.